Studies of hydrogen dynamics and structural aspects of polymer dispersed and boron added $MmNi_{3.5}Al_{0.5}Fe_{0.5}Co_{0.5}$

2005 J. Phys.: Condens. Matter 17 7531

(http://iopscience.iop.org/0953-8984/17/48/007)

INSTITUTE OF PHYSICS PUBLISHING JOURNAL OF PHYSICS: CONDENSED MATTER

J. Phys.: Condens. Matter **17** (2005) 7531–7546 doi:10.1088/0953-8984/17/48/007

Studies of hydrogen dynamics and structural aspects of polymer dispersed and boron added $MmNi_{3.5}Al_{0.5}Fe_{0.5}Co_{0.5}$

A Leela Mohana Reddy and S Ramaprabhu[1]

Alternative Energy Technology Laboratory, Department of Physics, Indian Institute of Technology Madras, Chennai-600 036, India

E-mail: ramp@iitm.ac.in

Received 18 August 2005, in final form 12 October 2005
Published 11 November 2005
Online at stacks.iop.org/JPhysCM/17/7531

Abstract

Pressure–composition (P–C) hydrogen absorption isotherms have been obtained for $MmNi_{3.5}Al_{0.5}Fe_{0.5}Co_{0.5}$ + 0.5 wt% B and $MmNi_{3.5}Al_{0.5}Fe_{0.5}Co_{0.5}$ + 25 wt% polyaniline (PANI) in the ranges 30–100 °C and 0.1–40 bar using a high pressure Seiverts' apparatus. The phase structure and microstructure morphologies of as-prepared and ball-milled materials have been analysed by XRD and SEM respectively. The effect of particle size, boron addition and PANI dispersion on the hydrogen absorption kinetics in $MmNi_{3.5}Al_{0.5}Fe_{0.5}Co_{0.5}$ has been studied and discussed. The diffusion coefficient and activation energy of dissolved hydrogen in $MmNi_{3.5}Al_{0.5}Fe_{0.5}Co_{0.5}$, $MmNi_{3.5}Al_{0.5}Fe_{0.5}Co_{0.5}$ + 0.5 wt% B and $MmNi_{3.5}Al_{0.5}Fe_{0.5}Co_{0.5}$ + 25 wt% PANI have been obtained from the studies of hydrogen absorption kinetics using the first order rate equation and the results have been discussed.

1. Introduction

Metal hydrides have drawn great interest from the research community due to their potential advantageous applications in the field of metal hydride based batteries, hydrogen storage for transportation, switchable mirrors, and heat pump applications [1–8]. Misch metal (Mm) based AB_5 alloys have been investigated in detail because of their low cost and large cyclic stability due to their low hydrogen decrepitation. However, the main disadvantage of Mm based alloys is their slow reaction sorption kinetics [9]. It has been shown that the addition of boron increases the discharge rate characteristics in $Mm(Ni_{0.64}Co_{0.2}Mn_{0.12}Al_{0.04})_x$ ($x = 4.5$–4.8) [10], increases the specific capacity in Ti_2Ni based electrodes [11], increases the cyclic stability in rare-earth-based hydrogen storage alloys [12] and enhances the activation

[1] Author to whom any correspondence should be addressed.

performance and rate capability of Mm based alloys [13, 14]. Since the hydrogen reaction sorption kinetics depends strongly on the oxide layers on the surface of the materials, polymers, which have catalytic action on chemical reactions, are found to enhance the reaction kinetics of hydrogen absorption in hydrogen storage materials [15]. Further, the improvement in hydrogen absorption kinetics with decrease in particle size has been studied in FeTi, Mg_2Ni and $LaNi_5$ alloys [16]. Recently, we have investigated the hydrogen storage properties of Zr based AB_2 alloys and Mm based AB_5 alloys for hydrogen storage applications [17–20]. The hydrogen absorption isotherms in polyaniline (PANI) dispersed and ball-milled Zr based AB_2 alloy $ZrMn_{0.85}Cr_{0.1}V_{0.05}Fe_{0.5}Ni_{0.5}$ show improved kinetics of hydrogen absorption [21]. In the present work, the effect of boron addition and PANI dispersion on the structure and the hydrogen absorption isotherms of Mm based AB_5 alloy $MmNi_{3.5}Al_{0.5}Fe_{0.5}Co_{0.5}$ have been systematically studied. In addition, the effect of reduction of particle size on the hydrogen absorption kinetics has been studied and the results have been discussed.

2. Experimental details

2.1. Sample preparation and characterization

$MmNi_{3.5}Al_{0.5}Fe_{0.5}Co_{0.5} + x$ wt% B ($x = 0, 0.5, 1.0, 2.0, 4.0, 5.0$) alloys have been prepared by arc melting the constituent elements in a stoichiometric ratio under argon atmosphere. The alloy buttons were re-melted six times by turning them upside down after each solidification to ensure homogeneity. During the preparation, the weight loss of the sample was less than 0.3%. Powder x-ray diffraction (XRD) patterns were taken with Cu Kα radiation, with Si as the standard (Shimadzu XD-D1 x-ray diffractometer).

2.2. Preparation of ball-milled and polymer dispersed materials

The arc melted alloys were milled for 4 h using a tungsten carbide vial and stainless steel balls in the planetary P5 ball mill. The milling was carried out at 300 rpm and ball to powder (B/P) mass ratio 10:1, under argon atmosphere. At selected intervals of time, small amounts of powder were successively taken from the mill for structural and morphological analysis. Polymer-dispersed crystalline materials have been prepared by milling the alloy particles with polyaniline in a 4:1 mass ratio, under argon atmosphere. The morphological characterizations of bulk, hydrogenated and polyaniline dispersed $MmNi_{3.5}Al_{0.5}Fe_{0.5}Co_{0.5}$ have been carried out using scanning electron microscopy (SEM; JEOL JSM 840A).

2.3. Hydrogen absorption isotherms and kinetic studies

Hydrogen absorption pressure–composition (P–C) isotherms and kinetics of hydrogen absorption have been studied by a conventional gasometric technique [22] using Seiverts' apparatus in the temperature and pressure ranges 30–100 °C and 0.1–30 bar respectively. The volume of gas contained in the sample cell at various pressures and temperatures in the absence of sample was precisely determined. At high pressures, the ideal gas law was corrected using the van der Waals equation for the volume of gas molecules and molecular interactions. Each time, about 0.5 g of sample was taken in the high pressure reactor and evacuated to 10^{-6} Torr. The sample was well activated by repeated hydrogenation and dehydrogenation, thus enabling the exposure of fresh surface for quantitative measurements. Before each cycle of hydrogen absorption, the alloys were degassed at 200 °C under a vacuum of 10^{-6} Torr for 3 h. The P–C isotherms were obtained by calculating the hydrogen concentration in the sample ($r = n_H/n_{f.u.}$) from the pressure drop during the absorption reaction at constant volume and

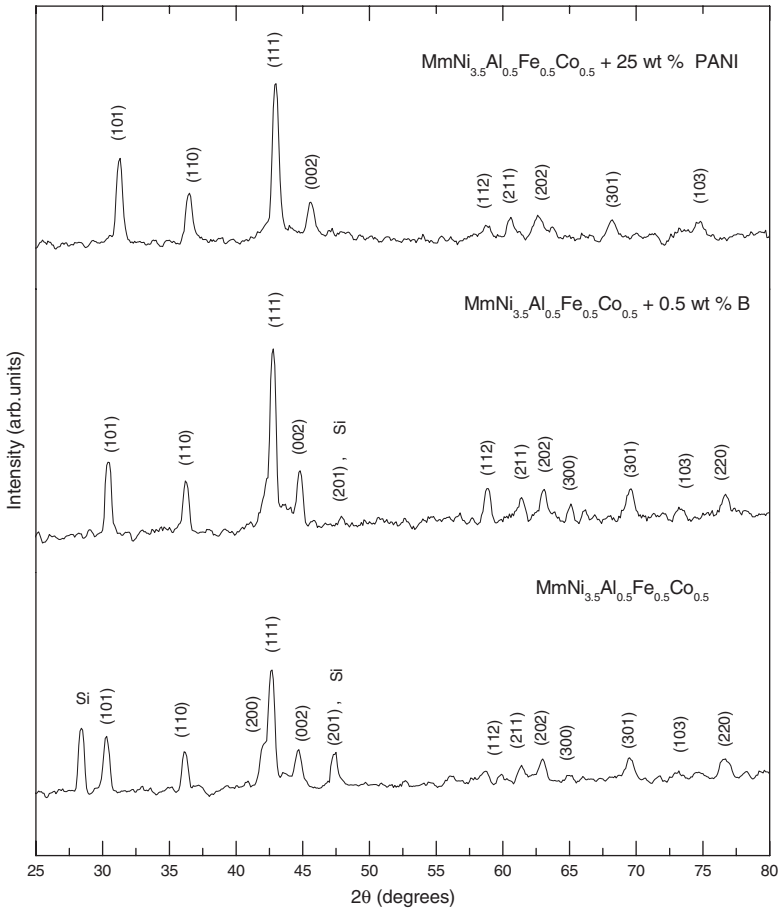

Figure 1. Powder x-ray diffractograms of $MmNi_{3.5}Al_{0.5}Fe_{0.5}Co_{0.5}$, $MmNi_{3.5}Al_{0.5}Fe_{0.5}Co_{0.5}$ + 0.5 wt% B and 4 h ball-milled $MmNi_{3.5}Al_{0.5}Fe_{0.5}Co_{0.5}$ + 25 wt% PANI.

constant temperature. The kinetics data were collected by recording the change in pressure as a function of time at constant temperature.

3. Results and discussion

3.1. Crystal structure

Room temperature Cu Kα powder XRD patterns confirm the single-phase nature in $MmNi_{3.5}Al_{0.5}Fe_{0.5}Co_{0.5}$ which crystallizes in $CaCu_5$ structure with space group $P6_3/mmm$. $MmNi_{3.5}Al_{0.5}Fe_{0.5}Co_{0.5} + x$ wt% B ($x = 0, 0.5$) alloys crystallize in $CaCu_5$ structure, whereas the alloys with 1.0, 2.0, 4.0 and 5.0 wt% B contain Fe_3B and $MmCo_4B$ secondary phases. These phases grow with increase in B content and the $CaCu_5$ parent phase disappears for alloys with 4 and 5 wt% of B (figure 1). The lattice constant and hence the unit cell volume of $MmNi_{3.5}Al_{0.5}Fe_{0.5}Co_{0.5}$ + 0.5 wt% B alloy is less than those of pure alloy. This reveals that the boron atoms directly occupy the substitutional sites instead of the interstitial sites as reported in C15 cubic Laves phase $Dy_{0.7}Pr_{0.3}Fe_2$ alloy [23]. Figure 2 shows the XRD

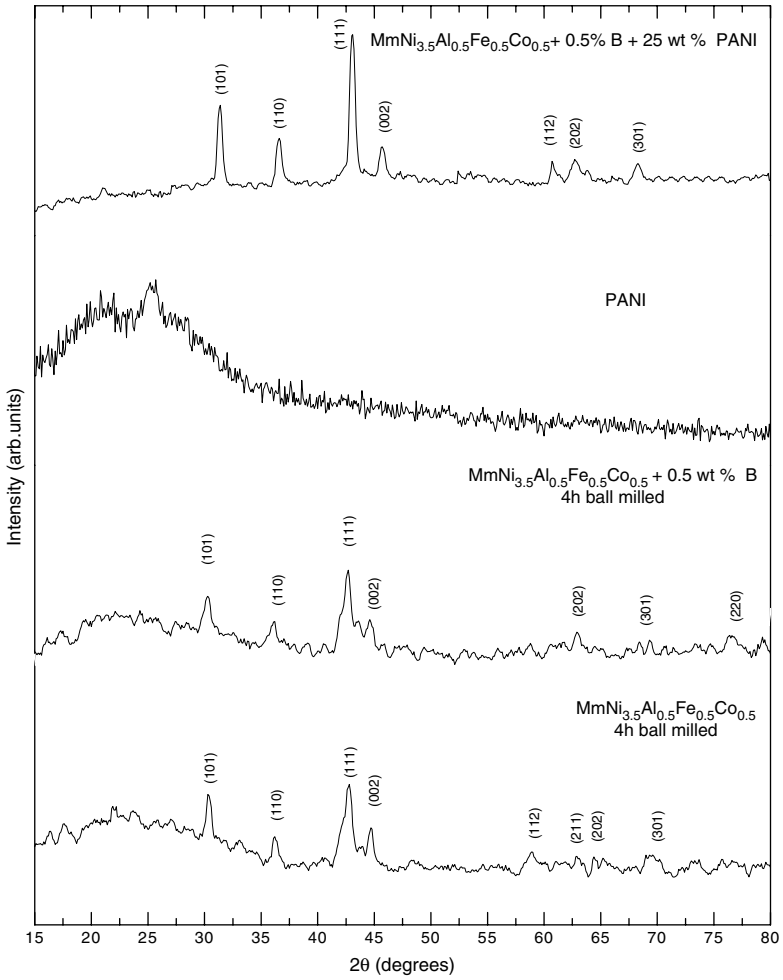

Figure 2. Powder x-ray diffractograms of 4 h ball-milled $MmNi_{3.5}Al_{0.5}Fe_{0.5}Co_{0.5}$, 4 h ball-milled $MmNi_{3.5}Al_{0.5}Fe_{0.5}Co_{0.5}$ + 0.5 wt% B, and $MmNi_{3.5}Al_{0.5}Fe_{0.5}Co_{0.5}$ + 0.5 wt% B + 25 wt% PANI ball milled for 4 h.

of 4 h ball-milled $MmNi_{3.5}Al_{0.5}Fe_{0.5}Co_{0.5}$ and $MmNi_{3.5}Al_{0.5}Fe_{0.5}Co_{0.5}$ + 0.5 wt% B. The decrease in the intensity of Bragg's reflections indicates a reduction in particle size upon ball milling. A single phase of hexagonal structure has been observed for polyaniline-dispersed $MmNi_{3.5}Al_{0.5}Fe_{0.5}Co_{0.5}$ and $MmNi_{3.5}Al_{0.5}Fe_{0.5}Co_{0.5}$ + 0.5 wt% B (figures 1 and 2). Figures 3(a)–(c) show the SEM images of as-melted $MmNi_{3.5}Al_{0.5}Fe_{0.5}Co_{0.5}$, after three hydrogen absorption/desorption cycles of $MmNi_{3.5}Al_{0.5}Fe_{0.5}Co_{0.5}$ and 4 h ball-milled $MmNi_{3.5}Al_{0.5}Fe_{0.5}Co_{0.5}$ + 25 wt% PANI. SEM images show the reduction in particle size upon ball milling. An average particle size of 5–10 μm has been observed for the alloy particles after ball milling. The SEM image of polyaniline dispersed $MmNi_{3.5}Al_{0.5}Fe_{0.5}Co_{0.5}$ material shows that the polyaniline is dispersed on the surface of the alloy particles.

3.2. P–C isotherms

Hydrogen absorption isotherms have been studied for $MmNi_{3.5}Al_{0.5}Fe_{0.5}Co_{0.5}$ + 0.5 wt% B and $MmNi_{3.5}Al_{0.5}Fe_{0.5}Co_{0.5}$ + 25 wt% PANI in the temperature and pressure ranges

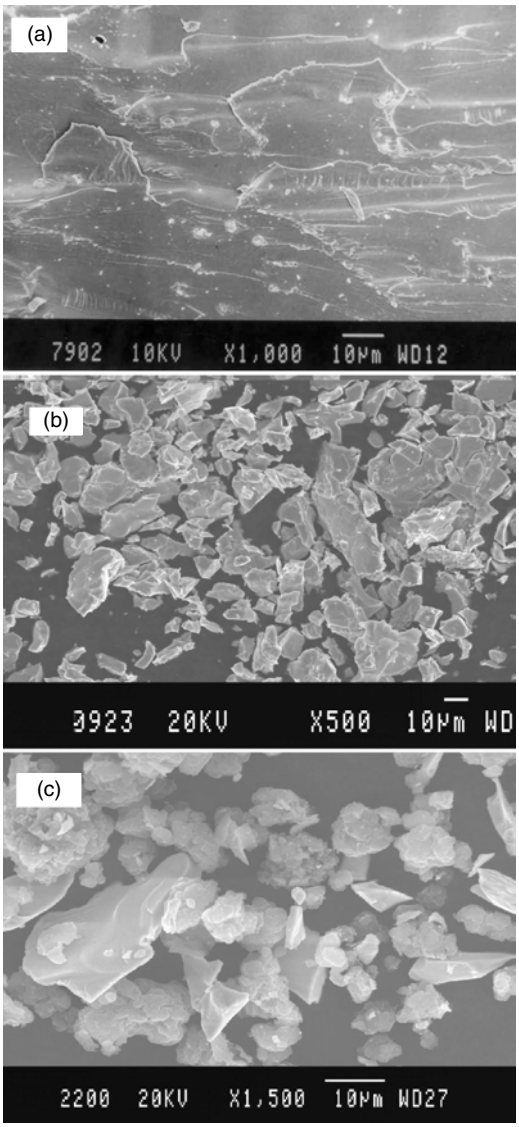

Figure 3. SEM image of (a) as-melted $MmNi_{3.5}Al_{0.5}Fe_{0.5}Co_{0.5}$, (b) after three hydrogen absorption/desorption cycles of $MmNi_{3.5}Al_{0.5}Fe_{0.5}Co_{0.5}$, and (c) 4 h ball-milled $MmNi_{3.5}Al_{0.5}Fe_{0.5}Co_{0.5}$ + 25 wt% PANI.

30–100 °C and 0.1–40 bar respectively and are shown in figure 4. These hydrogen absorption isotherms indicate the presence of two single-phase regions (α and β) and one two-phase region ($\alpha + \beta$) in the temperature and pressure ranges studied. A maximum hydrogen storage capacity of around 4.8 hydrogen atoms per formula unit has been obtained at 27 bar and 30 °C in $MmNi_{3.5}Al_{0.5}Fe_{0.5}Co_{0.5}$ + 0.5 wt% B. The hydrogen plateau pressure of the hydrogen absorbing alloy strongly depends on its unit cell volume of the alloy [17–21]. In the present work, at any particular temperature, the plateau pressure increases with the inclusion of boron due to contraction in unit cell volume. This can be attributed to the increase in the strain energy necessary to insert hydrogen atoms in the smaller interstitial sites of the

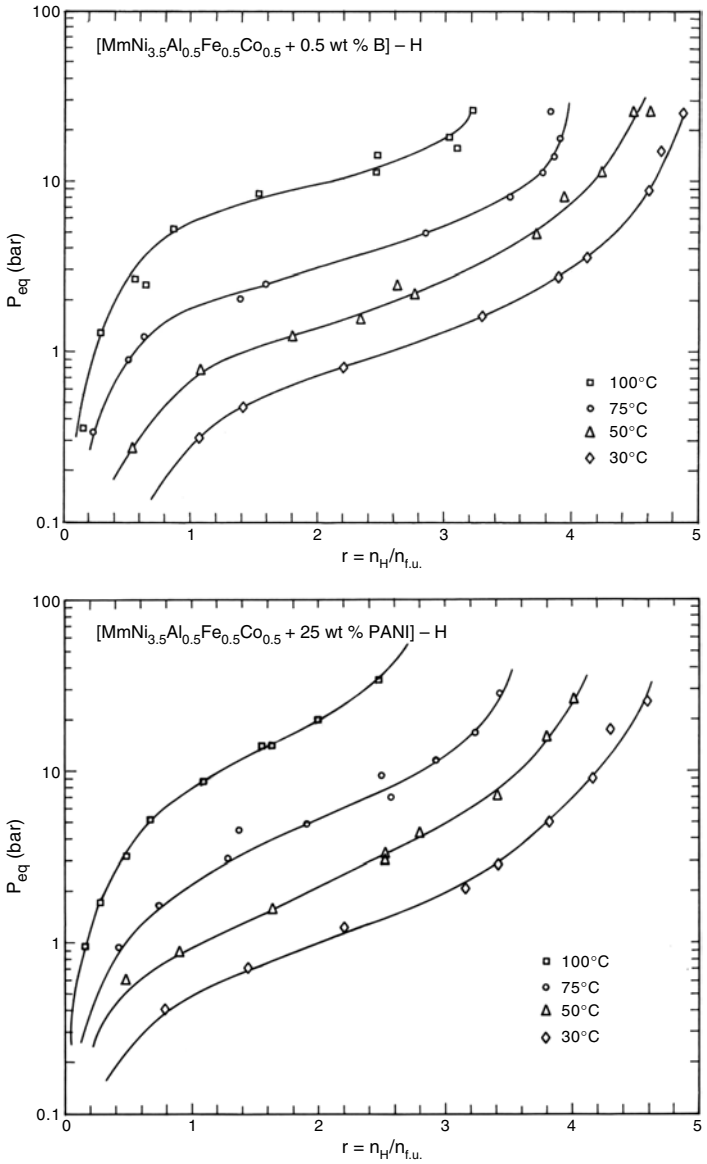

Figure 4. Hydrogen absorption isotherms of $MmNi_{3.5}Al_{0.5}Fe_{0.5}Co_{0.5}$ + 0.5 wt% B and $MmNi_{3.5}Al_{0.5}Fe_{0.5}Co_{0.5}$ + 25 wt% PANI.

$MmNi_{3.5}Al_{0.5}Fe_{0.5}Co_{0.5}$ + 0.5 wt% B. Further, at any particular pressure and temperature, the hydrogen concentration in $MmNi_{3.5}Al_{0.5}Fe_{0.5}Co_{0.5}$ + 25 wt% PANI is less compared to $MmNi_{3.5}Al_{0.5}Fe_{0.5}Co_{0.5}$ + 0.5 wt% B due to the fact that the polyaniline does not participate in the hydrogen absorption process.

3.3. Thermodynamics of dissolved hydrogen

From the hydrogen absorption isotherms, the relative partial molar enthalpy (ΔH_H) and the relative partial molar entropy (ΔS_H) of dissolved hydrogen can be obtained at a particular hydrogen concentration from the van't Hoff equation [24]:

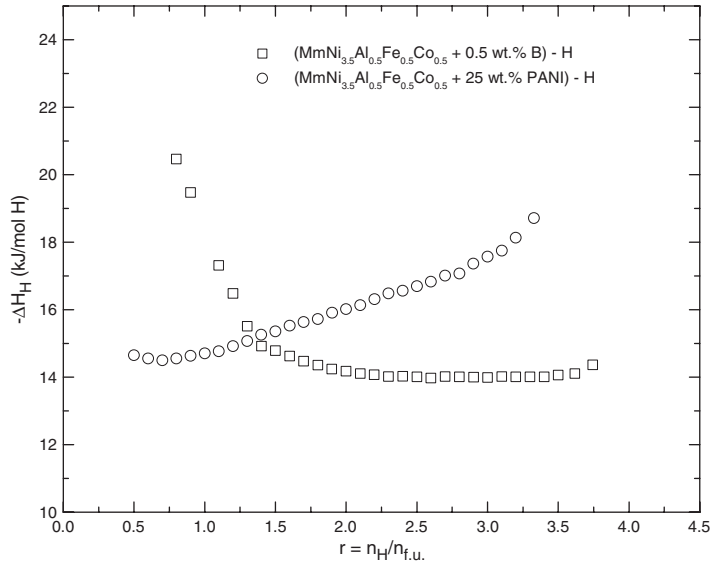

Figure 5. The dependence of ΔH_H on the hydrogen concentration in [$MmNi_{3.5}Al_{0.5}Fe_{0.5}Co_{0.5}$ + 0.5 wt% B]–H and [$MmNi_{3.5}Al_{0.5}Fe_{0.5}Co_{0.5}$ + 25 wt% PANI]–H.

Table 1. Lattice parameters and unit cell volume for $MmNi_{3.5}Al_{0.5}Fe_{0.5}Co_{0.5} + x$ wt% B ($x = 0, 0.5$) and their hydrides with accuracies of 0.002 Å and 0.1 Å^3 respectively.

Alloy	a (Å)	c (Å)	v (Å^3)
$MmNi_{3.5}Al_{0.5}Fe_{0.5}Co_{0.5}$	4.978	4.058	87.1
$MmNi_{3.5}Al_{0.5}Fe_{0.5}Co_{0.5}$ + 0.5 wt% B	4.973	4.053	86.8
[$MmNi_{3.5}Al_{0.5}Fe_{0.5}Co_{0.5}$ + 0.5 wt% B]–H_4	5.181	4.120	95.7
[$MmNi_{3.5}Al_{0.5}Fe_{0.5}Co_{0.5}$ + 25 wt% PANI]–$H_{3.8}$	5.218	4.150	97.8

$$\ln P_{H_2} = 2\left(\frac{\Delta H_H}{RT} - \frac{\Delta S_H}{R}\right) \tag{1}$$

ΔH_H and ΔS_H for dissolved hydrogen for a particular hydrogen concentration have been obtained by a least squares technique from the slope and intercepts of $\ln P_{H_2}$ versus $1/T$ plots, respectively, and the variation of ΔH_H with the hydrogen concentration is shown in figure 5. The Gibbs free energy ($\Delta\mu_H = \Delta H_H - T\Delta S_H$) at 30 and 50 °C, along with ΔH_H and ΔS_H, are listed in table 2. The dependence of $\Delta\mu_H$ on the unit cell volume for the alloys (tables 1, 2) suggests that the strain energy necessary to insert the hydrogen atoms increases with decrease in the unit cell volume of the alloy.

3.4. Hydrogen absorption kinetics

Figure 6 shows the hydrogen absorption kinetics of $MmNi_{3.5}Al_{0.5}Fe_{0.5}Co_{0.5}$, $MmNi_{3.5}Al_{0.5}Fe_{0.5}Co_{0.5}$ + 0.5 wt% B and $MmNi_{3.5}Al_{0.5}Fe_{0.5}Co_{0.5}$ + 25 wt% PANI alloys respectively at 30, 50, 75 and 100 °C. The kinetics graphs for these alloys show that the hydrogen concentration, r, increases with time and reaches an equilibrium value. This corresponds to an experimental point in the P–C isotherm of the corresponding alloy. The rate of absorption of hydrogen

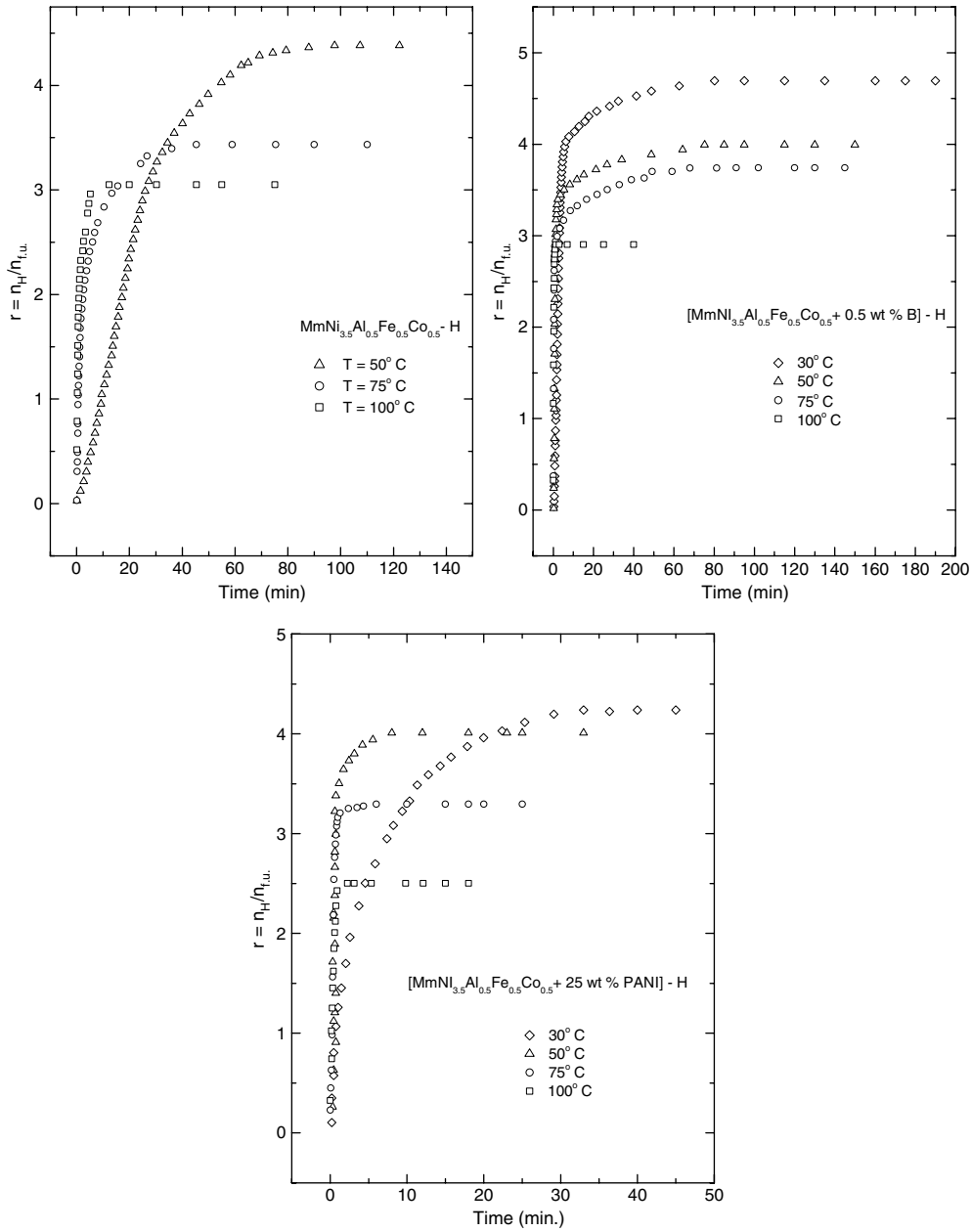

Figure 6. Kinetics of hydrogen absorption of $MmNi_{3.5}Al_{0.5}Fe_{0.5}Co_{0.5}$–H, [$MmNi_{3.5}Al_{0.5}Fe_{0.5}Co_{0.5}$ + 0.5 wt% B]–H and [$MmNi_{3.5}Al_{0.5}Fe_{0.5}Co_{0.5}$ + 25 wt% PANI]–H in the temperature range 30–100 °C.

is controlled by different mechanisms as the reaction proceeds through different regions. The different mechanisms are (a) surface process corresponding to the α phase, (b) interface process corresponding to the $(\alpha + \beta)$ phase and (c) the diffusion process corresponding to the β phase. During the initial stage of absorption, the surface process, chemisorptions and

Table 2. The equilibrium pressure, plateau slope, $\Delta H_H^{\alpha\to\beta}$, $\Delta S_H^{\alpha\to\beta}$ and $\Delta\mu_H^{\alpha\to\beta}$ for alloy hydrides at $r = n_H/n_{f.u.} = 2.0$.

Alloy hydrides	Equilibrium pressure (bar) 30 °C	50 °C	Plateau slope[a]	$-\Delta H_H^{\alpha\to\beta}$ (kJ/mol H)	$-\Delta S_H^{\alpha\to\beta}$ (J/K/mol H)	$\Delta\mu_H^{\alpha\to\beta}$ (kJ/mol H) 30 °C	50 °C
$MmNi_{3.5}Al_{0.5}Fe_{0.5}Co_{0.5}$–H[b]	0.83	1.61	1.4	16.8 ± 0.1	54.7 ± 0.2	−0.27	0.82
($MmNi_{3.5}Al_{0.5}Fe_{0.5}Co_{0.5}$ + 0.5 wt% B)–H	0.73	1.41	2.4	14.3 ± 0.3	46.0 ± 0.3	−0.4	0.5
($MmNi_{3.5}Al_{0.5}Fe_{0.5}Co_{0.5}$ + 25 wt% PANI)–H	1.0	2.13	2.6	16.2 ± 0.2	53.4 ± 0.5	0.0	1.0

[a] $\ln[P_{H/f.u.} = 4.0/P_{H/f.u.} = 1.0]$.
[b] Reference [19].

nucleation of hydride take place. As the absorption proceeds further, the hydride phase nuclei starts growing. At one stage, the growing hydride phase nuclei overlap with each other with a corresponding decrease in the interface area. In this process, the reaction rate is controlled by the phase transformation at the $(\alpha + \beta)$ interface. When the β-phase hydride is formed completely, hydrogen atoms probably get redistributed in the hydride phase and hence, diffusion of hydrogen seems to be the rate-determining step in the β phase [25, 26].

The reaction mechanism is analysed by comparing the observed rate with the Avrami–Erofeev type of equation [27]

$$F = 1 - e^{-Bt^m}. \tag{2}$$

The rate equation which best fits the observed data can be found for the appropriate value of m. For the present systems, the reaction order was determined as 1.0 for all phases by fitting the experimental data to the following equation:

$$-\ln\left(1 - \frac{m - m_0}{m_\infty - m_0}\right) = -\ln(1 - F) = kt \tag{3}$$

where F is the equilibrium rate which is $\frac{m}{m_\infty}$ for $m_0 = 0$ at $t = 0$. To obtain reaction constants k using equation (3), the results of hydrogen absorption process for various constant temperatures are plotted as $-\ln(1 - F)$ versus t (figure 7). It is seen from figure 7 that the experimental data fit to different linear segments and a gradual slope change occurs. This implies that different processes are controlling the rate, at initial and final stages of the absorption reaction. It is found from the P–C isotherms that the concentration at which the slope changes corresponds to the α phase to $(\alpha + \beta)$ phase and $(\alpha + \beta)$ phase to β phase transition region [28]. The rate constants (k) have been calculated for the different phases, at various temperatures from the slopes of the linear region of the fit shown in figure 7. The activation energy E_a can be calculated from the temperature dependence of the rate constant

$$k = k_0 \exp\left(-\frac{E_a}{k_B T}\right). \tag{4}$$

Figure 8 shows the Arrhenius plots of $\ln k$ versus $1/T$ for the interface processes $(\alpha+\beta)$ and $\ln D$ versus $1/T$ for diffusion process (β) respectively for these alloy hydrides, and from the slope a relative activation energy (E_a) is obtained. It is also possible to determine the diffusion coefficient (D) from the rate constant of the diffusion controlled reaction. The hydrogen diffusion coefficient can be obtained for the hydrogen content m_t at time t with spherical

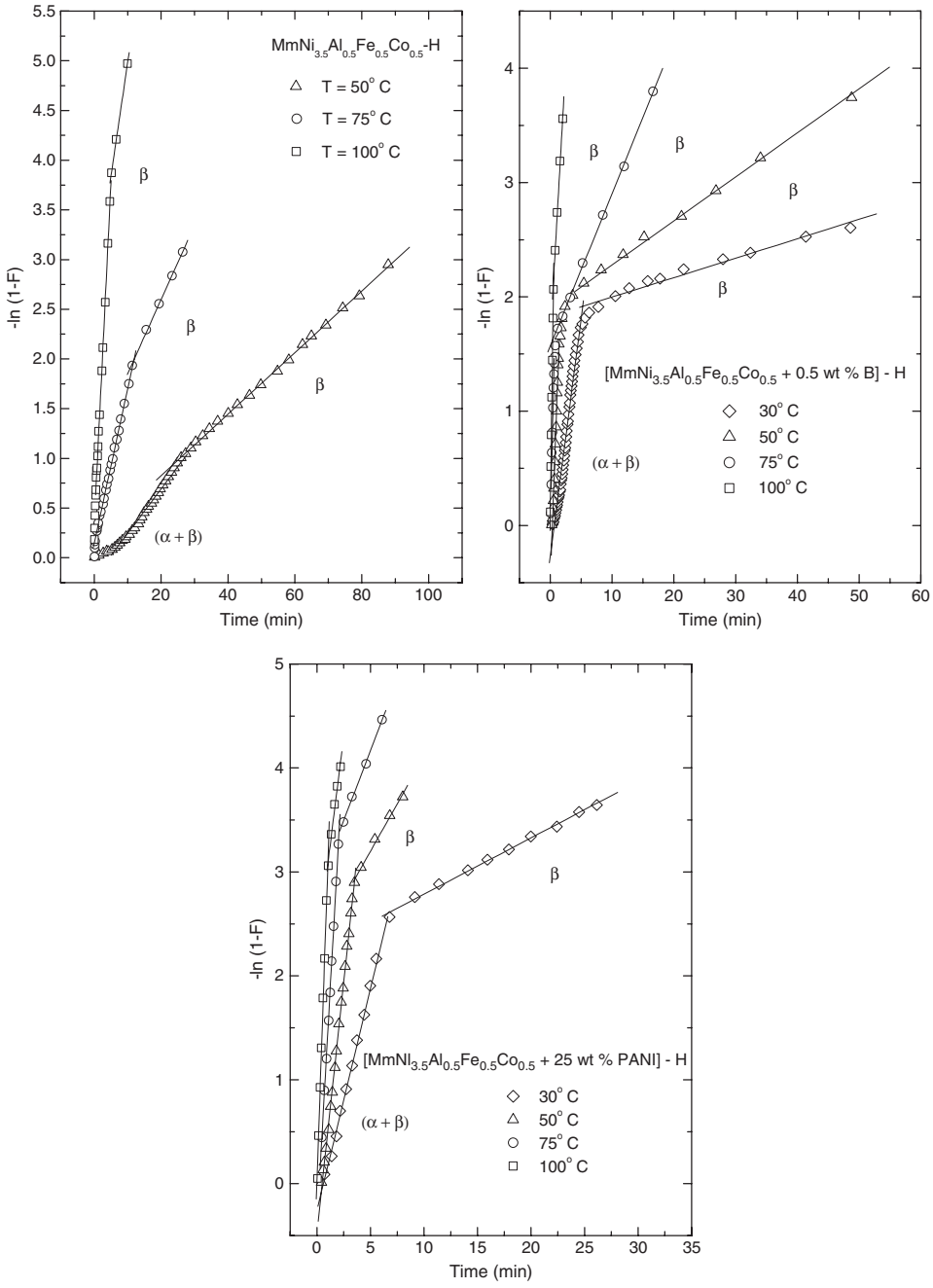

Figure 7. $-\ln(1-F)$ versus t plots for $MmNi_{3.5}Al_{0.5}Fe_{0.5}Co_{0.5}$–H, [$MmNi_{3.5}Al_{0.5}Fe_{0.5}Co_{0.5}$ + 0.5 wt% B]–H and [$MmNi_{3.5}Al_{0.5}Fe_{0.5}Co_{0.5}$ + 25 wt% PANI]–H in the temperature range 30–100 °C.

particle of radius r, from the first term of the series expansion of Fick's second law [29, 30].

$$1 - \frac{m_t}{m_\infty} = \frac{6}{\pi^2} \sum_{l=1}^{\infty} \frac{1}{l^2} \exp\left(\frac{-l^2 \pi^2 Dt}{r^2}\right). \tag{5}$$

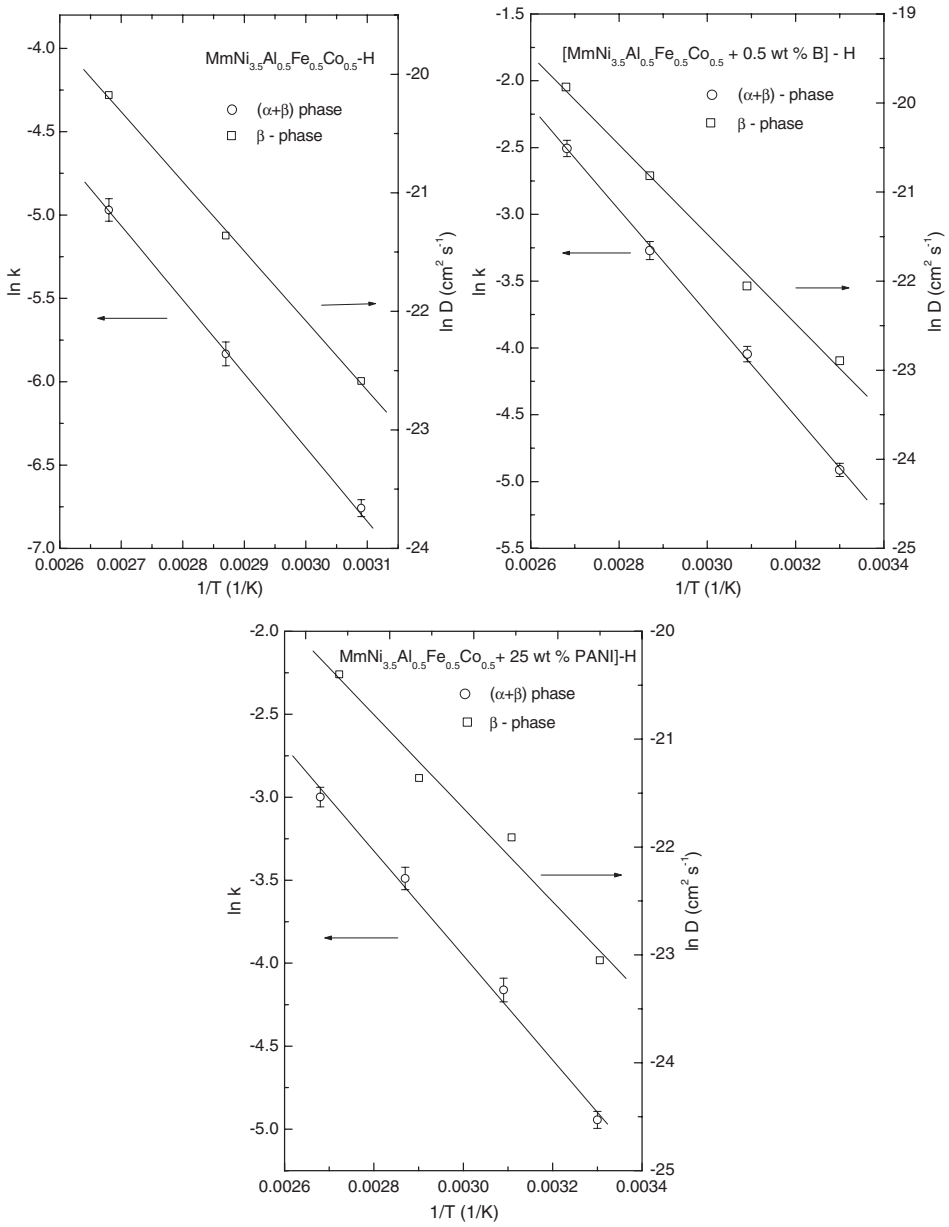

Figure 8. $\ln k$ versus $1/T$ plot in $(\alpha + \beta)$ phase and $\ln D$ versus $1/T$ plot in β phase for $MmNi_{3.5}Al_{0.5}Fe_{0.5}Co_{0.5}$–H, $[MmNi_{3.5}Al_{0.5}Fe_{0.5}Co_{0.5}$ + 0.5 wt% B]–H and $[MmNi_{3.5}Al_{0.5}Fe_{0.5}Co_{0.5}$ + 25 wt% PANI]–H.

For sufficiently long times, all except the $l = 1$ term can be neglected and the solution is

$$1 - F = \frac{6}{\pi^2} \exp\left(\frac{-\pi^2 Dt}{r^2}\right)$$
$$1 - F = \frac{6}{\pi^2} \exp(-K_D t) \tag{6}$$

where $K_D = \frac{\pi^2 D}{r^2}$.

Table 3. The activation energy and diffusion coefficients for $MmNi_{3.5}Al_{0.5}Fe_{0.5}Co_{0.5}$–H, [$MmNi_{3.5}Al_{0.5}Fe_{0.5}Co_{0.5}$ + 0.5 wt% B]–H and [$MmNi_{3.5}Al_{0.5}Fe_{0.5}Co_{0.5}$ + 25 wt% PANI]–H.

Sample	E_a (meV) ($\alpha + \beta$) phase	E_a (meV) β phase	D_0 ($cm^2\ s^{-1}$)	D ($cm^2\ s^{-1}$) 50 °C
$MmNi_{3.5}Al_{0.5}Fe_{0.5}Co_{0.5}$–H	382 ± 5	506 ± 10	1.1×10^{-2}	1.5×10^{-10}
[$MmNi_{3.5}Al_{0.5}Fe_{0.5}Co_{0.5}$ + 0.5 wt% B]–H	324 ± 10	433 ± 8	1.7×10^{-3}	2.6×10^{-10}
[$MmNi_{3.5}Al_{0.5}Fe_{0.5}Co_{0.5}$ + 25 wt% PANI]–H	268 ± 20	331 ± 12	7.4×10^{-5}	3.0×10^{-10}

Table 4. Time required for ball-milled, boron added and polyaniline dispersed $MmNi_{3.5}Al_{0.5}Fe_{0.5}Co_{0.5}$ materials to reach absorption kinetics equilibrium at 50 and 75 °C.

	Time (min)	
Sample	50 °C	75 °C
$MmNi_{3.5}Al_{0.5}Fe_{0.5}Co_{0.5}$	110	45
$MmNi_{3.5}Al_{0.5}Fe_{0.5}Co_{0.5}$ + 0.5 wt% B	75	49
$MmNi_{3.5}Al_{0.5}Fe_{0.5}Co_{0.5}$ (4 h ball milled)	37	16
$MmNi_{3.5}Al_{0.5}Fe_{0.5}Co_{0.5}$ + 0.5 wt% B (4 h ball milled)	32	12
$MmNi_{3.5}Al_{0.5}Fe_{0.5}Co_{0.5}$ + 25 wt% PANI	8	6
$MmNi_{3.5}Al_{0.5}Fe_{0.5}Co_{0.5}$ + 0.5 wt% B + 25 wt% PANI	10	5

Hence, by measuring the hydrogen content as a function of time (m_t) and the equilibrium hydrogen content m_α at a particular temperature, one can calculate the diffusion coefficient of hydrogen. The diffusion coefficients have been calculated from the slope of linear fitting corresponding to the β phase (see figure 7) using an average particle size of 20 μm for hydrogenated $MmNi_{3.5}Al_{0.5}Fe_{0.5}Co_{0.5}$ and $MmNi_{3.5}Al_{0.5}Fe_{0.5}Co_{0.5}$ + 0.5 wt% B and 10 μm for 4 h ball-milled $MmNi_{3.5}Al_{0.5}Fe_{0.5}Co_{0.5}$ + 25% PANI (see figure 3). The diffusion coefficients of hydrogen in the investigated temperature range for $MmNi_{3.5}Al_{0.5}Fe_{0.5}Co_{0.5}$–H, [$MmNi_{3.5}Al_{0.5}Fe_{0.5}Co_{0.5}$ + 0.5 wt% B]–H and [$MmNi_{3.5}Al_{0.5}Fe_{0.5}Co_{0.5}$ + 25 wt% PANI]–H are comparable with the value of 2.55×10^{-10} $cm^2\ s^{-1}$ at 30 °C for $MmNi_{3.8}Al_{0.4}Fe_{0.4}Co_{0.4}$–H obtained by hydrogen absorption kinetics [19]. Activation energies (E_a) calculated from the slope of the Arrhenius plot (figure 8) in the (α + β) phase and β phase for $MmNi_{3.5}Al_{0.5}Fe_{0.5}Co_{0.5}$–H, [$MmNi_{3.5}Al_{0.5}Fe_{0.5}Co_{0.5}$ + 0.5 wt% B]–H and [$MmNi_{3.5}Al_{0.5}Fe_{0.5}Co_{0.5}$ + 25 wt% PANI]–H are listed in table 3. Figure 9 shows the comparison of hydrogen absorption kinetics in $MmNi_{3.5}Al_{0.5}Fe_{0.5}Co_{0.5}$, $MmNi_{3.5}Al_{0.5}Fe_{0.5}Co_{0.5}$ + 0.5 wt% B, $MmNi_{3.5}Al_{0.5}Fe_{0.5}Co_{0.5}$ + 25 wt% PANI, $MmNi_{3.5}Al_{0.5}Fe_{0.5}Co_{0.5}$ + 0.5 wt% B + 25 wt% PANI, 4 h ball-milled $MmNi_{3.5}Al_{0.5}Fe_{0.5}Co_{0.5}$ and 4 h ball-milled $MmNi_{3.5}Al_{0.5}Fe_{0.5}Co_{0.5}$ + 0.5 wt% B alloys at 50 and 75 °C respectively. The time required to reach the hydrogen equilibrium (P_{eq}) at 50 °C in polyaniline dispersed $MmNi_{3.5}Al_{0.5}Fe_{0.5}Co_{0.5}$ is around 10 min, compared to 110 min in pure alloy (see table 4). In Zr based $ZrMn_{0.85}Cr_{0.1}V_{0.05}Fe_{0.5}Ni_{0.5}$ + 1 wt% B alloy, the time required to reach P_{eq} at 50 °C is 76 min in polyaniline dispersed alloy compared to 95 min in parent alloy at the same initial hydrogen pressure [21]. Thus the effect of polyaniline dispersion on hydrogen absorption kinetics is more prominent in AB_5 alloys rather than in AB_2 alloys, due to the presence of active rare earths in AB_5 alloys. Thus polyaniline is an excellent catalyst for improving the reaction kinetics of Mm based AB_5 alloy. Further work is in progress to verify the catalytic activity of polyaniline for hydrogen absorption kinetics in other Mm based AB_5 alloys.

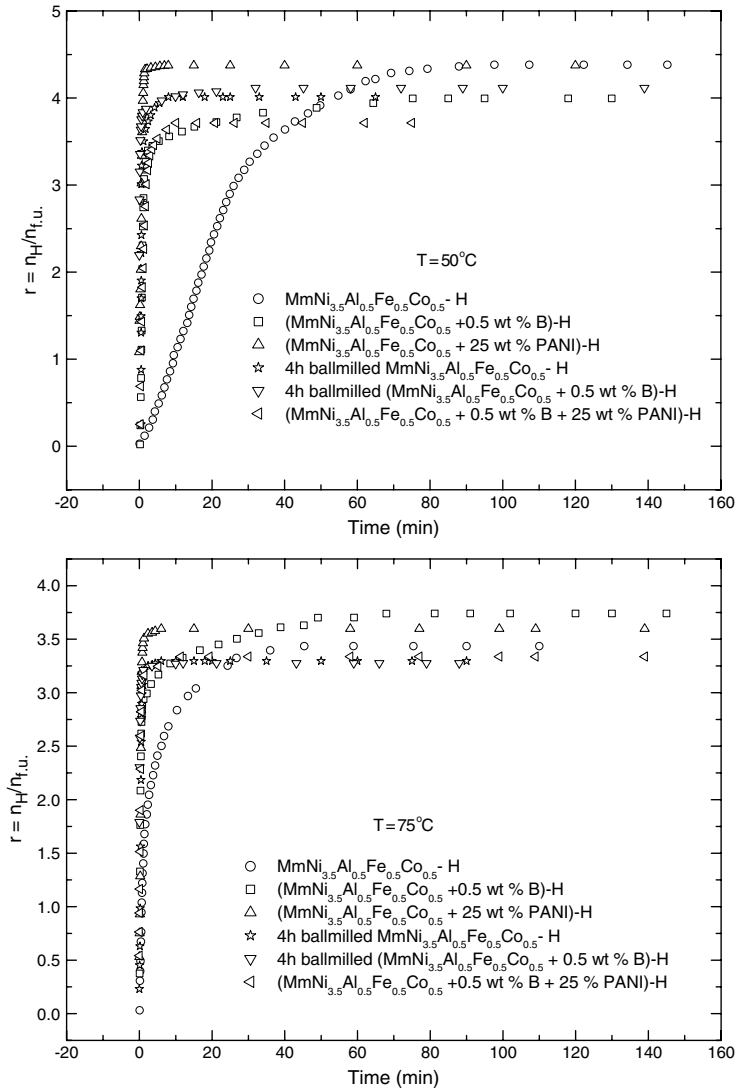

Figure 9. Kinetics of hydrogen absorption in ball-milled, boron added and polyaniline dispersed $MmNi_{3.5}Al_{0.5}Fe_{0.5}Co_{0.5}$ at 50 and 75 °C.

3.5. X-ray diffractograms of alloy hydrides

Change in crystal structure from hexagonal to orthorhombic has been observed with hydrogenation of $SmCo_5$ and $PrCo_5$ [31, 32]. However, C14 hexagonal type AB_2 alloys such as $ZrMnFe_{0.5}Ni_{0.5}$ and $PuNi_3$ type AB_3 alloys such as $ErFe_3$ and YFe_3 and $Zr_xTb_{1-x}Fe_3$ retain their structure upon hydrogenation [17, 33–36]. Further, hydrogenation on $LaNi_5$, $LaNi_{1-x}M_x$ ($M = Mn, Cu, Al, Fe$; $x = 0.25, 0.50$) and $MmNi_{4.2}Al_{0.8}$ show no structural change with increase in cell volume [37, 38]. Figure 10 shows the powder XRD for $[MmNi_{3.5}Al_{0.5}Fe_{0.5}Co_{0.5}$ + 0.5 wt% B]–$H_{3.8}$ and $[MmNi_{3.5}Al_{0.5}Fe_{0.5}Co_{0.5}$ + 25 wt% PANI]–$H_{4.0}$. The powder XRD patterns show that there is no structural change upon hydrogenation and the Bragg reflections are identical to that of the

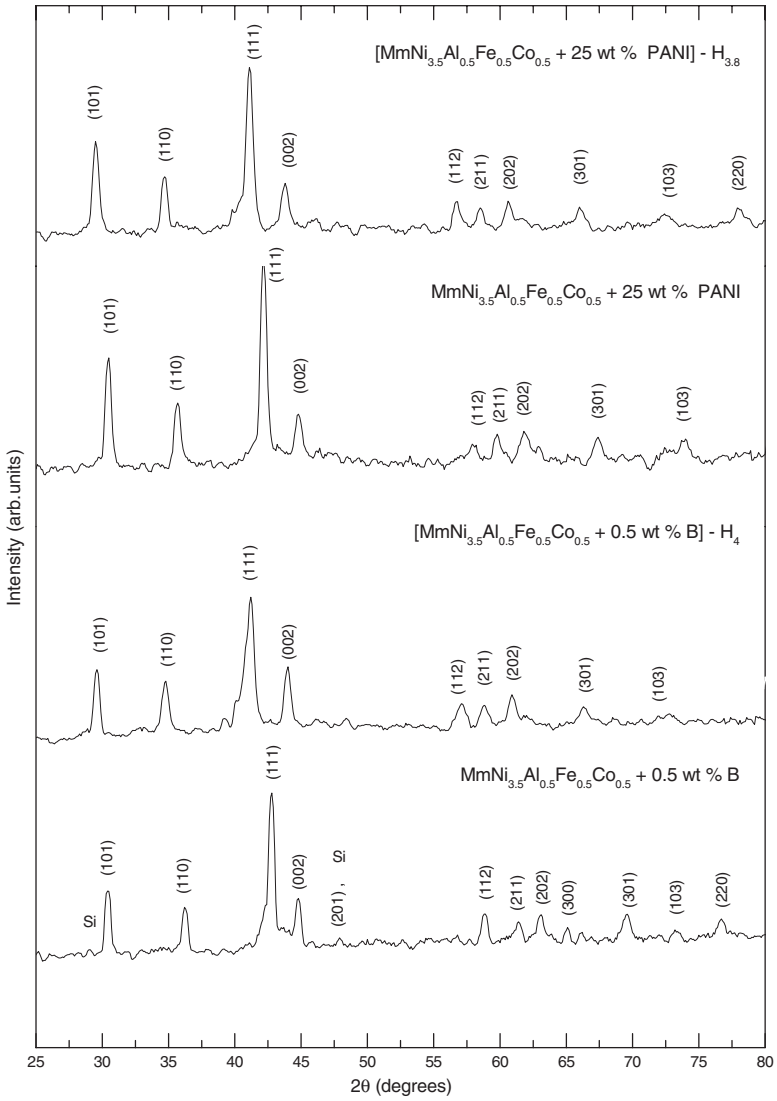

Figure 10. Powder x-ray diffractograms of hydrides of $MmNi_{3.5}Al_{0.5}Fe_{0.5}Co_{0.5}$ + 0.5 wt% B and $MmNi_{3.5}Al_{0.5}Fe_{0.5}Co_{0.5}$ + 25 wt% PANI.

parent alloy with increase in the unit cell volume. The unit cell volume expansion is around 10% in $MmNi_{3.5}Al_{0.5}Fe_{0.5}Co_{0.5}$ + 0.5 wt% B and $MmNi_{3.5}Al_{0.5}Fe_{0.5}Co_{0.5}$ + 25 wt% PANI.

4. Conclusions

$MmNi_{3.5}Al_{0.5}Fe_{0.5}Co_{0.5} + x$ wt% B ($x = 0, 0.5$) alloys crystallize in $CaCu_5$ structure, whereas the alloys with 1.0, 2.0, 4.0 and 5.0 wt% B contain Fe_3B and $MmCo_4B$ secondary phases. These phases grow with increase in B content and the $CaCu_5$ parent phase disappears for alloys with 4 and 5 wt% of B. The hydrogen absorption isotherms of $MmNi_{3.5}Al_{0.5}Fe_{0.5}Co_{0.5}$ + 0.5 wt% B show that with the inclusion of boron the hydrogen storage capacity decreases and plateau

pressure increases due to the contraction of unit cell volume. This is attributed to the increase in the strain energy necessary to insert hydrogen atoms in the smaller interstitial sites. The reaction kinetics of hydrogen absorption increases with inclusion of boron. Polymer dispersed and 4 h ball-milled alloys show rapid kinetics of hydrogen absorption when compared to the parent alloy. Polyaniline is found to be an excellent catalyst for improving the hydrogen reaction kinetics in the present system. The diffusion coefficient of hydrogen has the activation energy $E = 506 \pm 10$, 433 ± 8 and 331 ± 12 meV and pre-exponential factor $D_0 = 1.1 \times 10^{-2}$, 1.6×10^{-3} and 7.4×10^{-5} $cm^2\ s^{-1}$ respectively for $MmNi_{3.5}Al_{0.5}Fe_{0.5}Co_{0.5}$–H, [$MmNi_{3.5}Al_{0.5}Fe_{0.5}Co_{0.5}$ + 0.5 wt% B]–H and [$MmNi_{3.5}Al_{0.5}Fe_{0.5}Co_{0.5}$ + 25 wt% PANI]–H. These materials do not undergo any structural change upon hydrogenation.

Acknowledgments

The authors are grateful to the DRDO, DST and MNES for the support of this work. One of the authors (ALMR) is grateful to IIT Madras for financial support.

References

[1] Kleparis J, Wojcik G, Czerwinski A, Skowronski J, Kopczyk M and Beltowska-Brzezinska M 2001 *J. Solid State Electrochem.* **5** 229
[2] Jurczyk M, Smardz L, Smardz K, Nowak M and Jankowska E 2003 *J. Solid State Chem.* **171** 30
[3] Griessen R, Huiberts J N, Kermers M, van Gogh A T M, Koeman H J, Dekker J P and Notten P H L 1997 *J. Alloys Compounds* **253/254** 44
[4] Huiberts J N, Rector R G J H, Wijngaaden R J, Dekker J P, de Groot D G and Koeman N J P 1996 *Nature* **380** 231
[5] Hsu S E, Beibutian V M and Yeh M T 2002 *J. Alloys Compounds* **330–332** 882
[6] Supper W, Groll M and Mayer U 1984 *J. Less-Common Met.* **104** 279
[7] Dantzer P and Meunier F 1988 *Mater. Sci. Forum* **31** 1
[8] Chernikov A S, Izhvanov L A, Solovey A I, Frolov V P and Shanin Yu I 2002 *J. Alloys Compounds* **330–332** 907
[9] Sastri M V C, Viswanathan B and Srinivasa Murthy S 1998 *Metal Hydrides* (New Delhi: Narosa Publishing House)
[10] Tadokoro M, Nogami M, Chikano Y, Kimoto M, Ise T, Nishio K and Furukawa N 1993 *J. Alloys Compounds* **192** 179
[11] Luan B, Cui N, Zhao H J, Liu H K and Dou S X 1996 *Int. J. Hydrog. Energy* **21** 373
[12] Hu W K, Ye Z and Noreus D 1998 *J. Alloys Compounds* **280** 314
[13] Ye H, Zhang H, Wu W Q and Huang T S 2000 *J. Alloys Compounds* **312** 68
[14] Ye H, Huang Y X, Huang T S and Zhang H 2002 *J. Alloys Compounds* **330–332** 866
[15] Wayde R 2001 *Schmidt Proc. 2001 DOE Hydrogen Program Review* NREL/CP-570-30535
[16] Aoyagi H, Aoki K and Masumoto T 1995 *J. Alloys Compounds* **231** 804
[17] Mani N, Sivakumar R and Ramaprabhu S 2002 *J. Alloys Compounds* **337** 148
[18] Mani N and Ramaprabhu S 2005 *Int. J. Hydrog. Energy* **30** 53
[19] Mani N and Ramaprabhu S 2004 *J. Alloys Compounds* **363** 275
[20] Mani N, Kesavan T R and Ramaprabhu S 2002 *J. Phys.: Condens. Matter* **14** 3939
[21] Leela Mohana Reddy A and Ramaprabhu S 2005 *Int. J. Hydrog. Energy* at press
[22] Sivakumar R 2000 *PhD Thesis* Indian Institute of Technology, Madras, India
[23] Ren W J, Zhang Z D, Liu J P, Zhao X G, Liu W, Geng D Y and Jin X M 2002 *J. Appl. Phys.* **91** 8207
[24] Flanagan T B and Park C N 1998 *Mater. Sci. Forum* **31** 297
[25] Ramesh R and Rama Rao K V S 1993 *J. Alloys Compounds* **191** 101
[26] Koh J T, Goudy A J, Huang P and Zhou G 1989 *J. Less-Common Met.* **153** 89
[27] Masuhiro Y and Etsuo A 1994 Ternary hydrides *Materials Science and Technology: A Comprehensive Treatment* (*Electronic and Magnetic properties of Metals and and Ceramics, Part-II*) vol 3B, ed R W Cahn, P Hassen and E J Kramer (New York: VCH) chapter 13
[28] Sivakumar R, Ramaprabhu S, Rama Rao K V S, Anton H and Schmidt P C 2000 *Int. J. Hydrog. Energy* **25** 463
[29] Crank J 1956 *Mathematics of Diffusion* (Fair Lawn, NJ: Oxford University Press)

[30] Jost W 1952 *Diffusion in Solids, Liquids and Gases* (New York: Academic)
[31] Goudy A, Wallace W E, Craig R S and Takeshita T 1978 *Thermodynamics and Kinetics of Hydrogen Absorption in Rare Earth–Iron Compounds* (*Advances in Chemistry Series* vol 167) ed R Bau (Washington, DC: American Chemical Society) p 312
[32] Oesterreicher H 1981 *Appl. Phys.* **24** 169
[33] Yvon K and Fischer P 1988 *Hydrogen in Intermetallic Compounds—I* (*Topics in Applied Physics* vol 63) ed L Schlapbach (Berlin: Springer) chapter 4, pp 112–3
[34] Malik S K, Pourarian F and Wallace W E 1983 *J. Magn. Magn. Mater.* **40** 27
[35] Buschow K H J 1976 *Solid State Commun.* **19** 421
[36] Sivakumar R, Ramaprabhu S, Rama Rao K V S, Anton H and Schmidt P C 1999 *J. Alloys Compounds* **285** 143
[37] Nakamura Y, Oguro K, Uehara I and Akiba E 2000 *J. Alloys Compounds* **298** 138
[38] Mungole M N and Balasubramaniam R 2000 *Int. J. Hydrog. Energy* **25** 55